Trans. JWRI, Vol. 22 (1993), No.1

Effects of Shielding Gas Composition on Metal Transfer Phenomena in High Current GMA Welding†

Masao USHIO*, Kenji IKEUCHI**, Manabu TANAKA*** and Takeshi SETO****

Abstract

Metal transfer phenomena in high current GMA welding with several kinds of shielding gas have been systematically investigated with high-speed cinecamera. Typical transfer modes are classified into four types, depending on the welding current: globular transfer, axial spray transfer, swinging spray transfer, and rotating spray transfer. The dependence of the transfer mode as welding current can be explained by the instability of melted electrode using numerical modeling based on MHD theory.

KEY WORDS: (GMA welding) (Shielding gas) (Metal transfer) (Melted electrode) (Instability)

1. Introduction

The high current GMA welding process is usually carried out using shielding gas of three or four-part gas mixture of Ar, He, CO_2 and O_2[1]. This process contributes to the improvement of welding efficiency by permitting to obtain a stable arc in high current region from 400 to 600A[2]. However, there have been only a few information about metal transfer phenomena in high current region, and so the role of gases constituting the shielding has not been understood well.

In the present investigation, therefore, we have observed systematically metal transfer phenomena in high current GMA welding with several kinds of shielding gas in order to understand the effects of shielding gas composition on the metal transfer.

2. Experimental Procedure

Experimental setup for observing the metal transfer phenomena during GMA welding is schematically shown in **Fig.1**. The metal transfer phenomena was recorded dynamically with a high-speed cinecamera (6000 frame/sec). A xenon lamp was used as back-light for the arc. The base metal was a mild steel plate ($500^{l}\times75^{w}\times6^{t}$mm). The welding wire was mild steel wire of 1.2mm diameter, JIS YCW-1. The shielding gas was Ar, He, Ar+CO_2, Ar+He and Ar+He+O_2. Mixture ratios of the shielding gas are shown in **Table 1.**

Welding conditions are tabulated in **Table 2.** A schematic diagram of torch structure is shown in **Fig.2.**

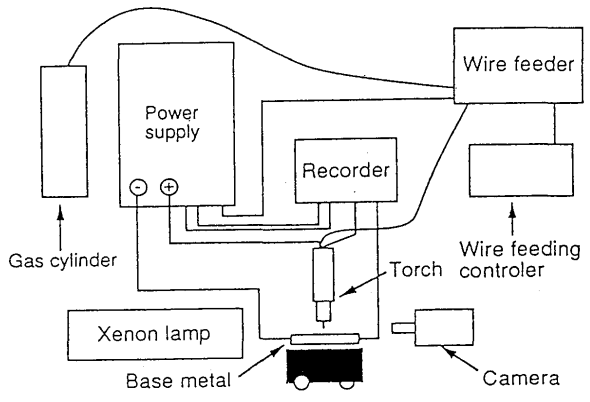

Fig.1 Schematic diagram of experimental setup.

† Recived on 30 July 1993
* Professor
** Associate Professor
*** Research Associate
**** Graduate Student

Transactions of JWRI is published by Welding Research Institute, Osaka University, Ibaraki, Osaka 567, Japan

Table 1 Mixture ratio of shielding gas.

(a) $Ar+CO_2$

Ar(%)	100	95	90	80	75	70	60
CO_2(%)	0	5	10	20	25	30	40

(b) Ar+He

Ar(%)	100	90	70	50	40	30	20	10	0
He(%)	0	10	30	50	60	70	80	90	100

(c)$Ar+He+O_2$

Ar(%)	89	85
He(%)	10	10
O_2(%)	1	5

Table 2 Welding conditions.

Wire fees rate	: max 33 m/min
Extension lenght	: 25 mm
Arc lenght	: 6 mm
Welding current	: 150-600 A
Welding speed	: 40 cm / min

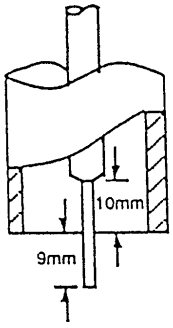

Fig.2 Schematic diagram of torch structure

3. Experimental Results and Discussion

3.1 $Ar+CO_2$ gas mixture for shielding

When $Ar+CO_2$ gas mixture is used for shielding, metal transfer modes are roughly classified into four types as schematically illustrated in Fig.3: globular transfer, axial spray transfer, swinging spray transfer and rotating spray transfer.

The globular transfer mode is characterized by the droplet diameter larger than the wire diameter. This mode is further classified into two types, i.e., drop transfer and repelled transfer as shown in Fig.3.

On the other hand, spray transfer, which is the general term for axial spray transfer, swinging spray transfer, and rotating spray transfer, is characterized by the droplet diameter smaller than the wire diameter.

The axial spray transfer is the mode in which the droplet directly transfers to the base metal. This mode is further classified into three types: projected transfer, streaming transfer and repelled spray transfer.

The rotating spray transfer is the mode in which the droplet is sprinkled on the base metal with stable rotation of the melted electrode.

Between the axial spray transfer and rotating spray transfer, we find a mode in which the droplet is scattered on the base metal with unstable swing of the electrode. This mode was named 'swinging spray transfer'. The swinging spray transfer is a precursory stage of the transition from axial spray transfer to rotating spray transfer.

The map of metal transfer modes is shown in Fig.4, when $Ar+CO_2$ gas mixture is used for shielding. These modes changed from globular transfer to rotating spray transfer via axial spray transfer and swinging spray transfer as the welding current was increased. There are transitional regions between globular transfer and axial spray transfer and between swinging spray transfer and rotating spray transfer.

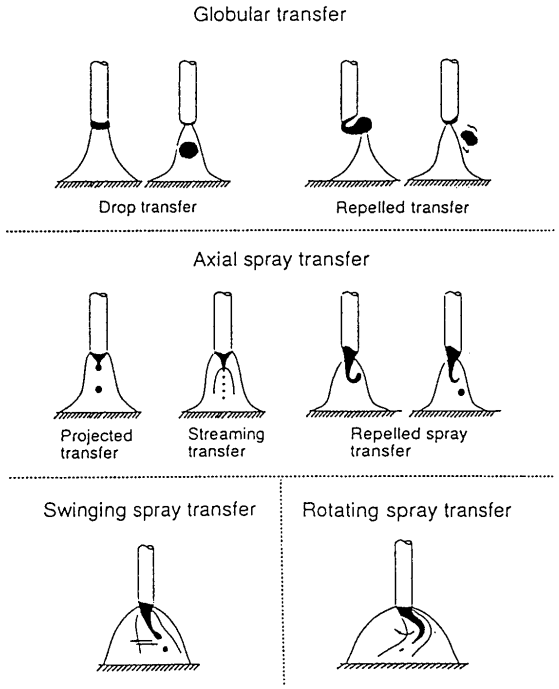

Fig.3 Schematic illustration of metal transfer modes.

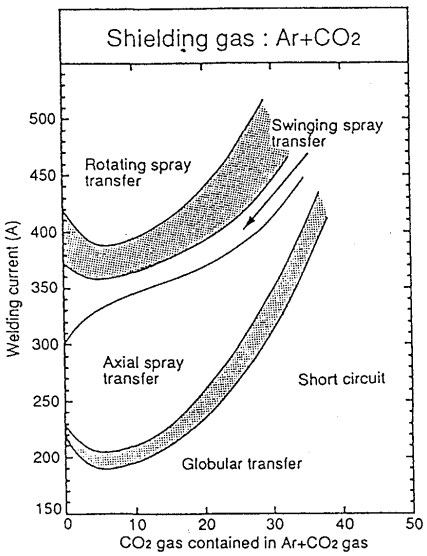

Fig.4 Map of metal transfer modes ($Ar+CO_2$).

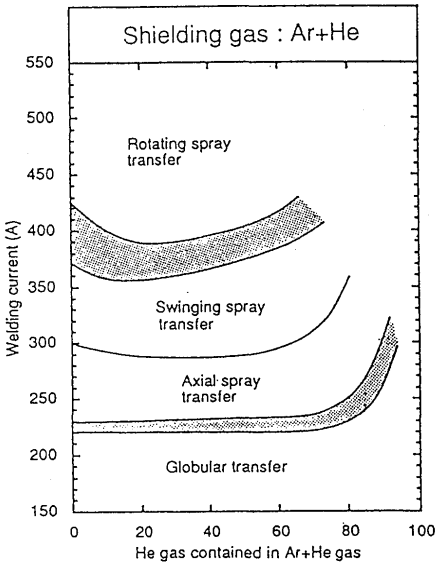

Fig.5 Map of metal transfer modes (Ar+He).

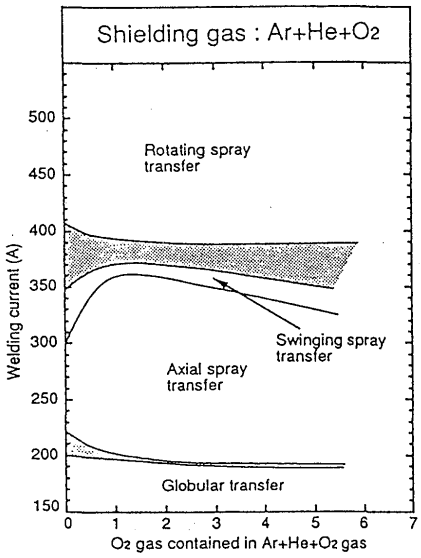

Fig.6 Map of metal transfer modes ($Ar+He+O_2$).

The welding current at the boundaries of these modes increased with the mixture ratio of CO_2, when the CO_2 ratio was more than about 5%. When the mixture ratio of CO_2 is 0~10%, only drop transfer mode was observed in the globular transfer region, and projected and streaming transfer modes were observed in the axial spray transfer region. On the other hand, when the mixture ratio of CO_2 exceeded 10%, the repelled transfer mode dominated the globular transfer region and the repelled spray transfer mode dominated the axial spray transfer region. Those results suggest that the introduction of CO_2 into shielding gas increased the arc force, which held up the melted electrode. The holding-up effect of the arc force led to the decrease in the effective length of the melted electrode. Probably for this reason, metal transfer mode associated with shorter melted electrode could dominate the high welding current region, as the mixture ratio of CO_2 was increased. We think this can explain why the welding current at the boundaries between the transfer modes was increased with the mixture ratio of CO_2.

3.2 Ar+He gas mixture for shielding

When Ar+He gas mixture is used for shielding, as shown in **Fig.5**, the globular, axial spray, swinging spray and rotating spray transfer mode were observed similarly to those shown in Fig.4. However, there are two characteristic points in this map as compared with Fig.4. One is that the welding current at the boundaries between transfer modes were almost independent of the mixture ratio of He from 0 to 70%. The other is that the areas of swinging spray transfer mode and rotating spray transfer mode were larger than those in Fig.4.

When the mixture ratio of He is 0~70%, the drop transfer mode dominated the globular transfer region, and the projected and streaming transfer modes dominated the axial spray transfer region. On the other hand, when the mixture ratio of He is over 70%, the repelled transfer mode dominated the globular transfer region and the repelled spray transfer mode dominated the axial spray transfer region.

The addition of He into the shielding gas significantly increased the length of the melted electrode contrary to CO_2.

3.3 Ar+He+O_2 gas mixture for shielding

When $Ar+He+O_2$ gas mixture is used for shielding, the map of metal transfer mode is shown in **Fig.6**. The globular, axial spray, swinging spray and rotating spray transfer mode appeared similarly to those in Figs.4 and 5. The introduction of O_2 into Ar+He gas mixture increased the area of axial spray transfer mode and decreased the area of swinging spray transfer mode.

The melted electrode was shortened with the increase in mixture ratio of O_2. The drop transfer mode dominated the globular transfer region, and the projected and streaming transfer modes dominated the axial spray transfer region. The length of the melted electrode was

observed to be decreased as the O_2 ratio was increased. It seems that the O_2 addition did not increase the arc force, since neither the repelled transfer or the repelled spray transfer was observed in this case. It has been generally accepted that the O_2 addition decreases the surface energy of the melted electrode[3]. Therefore, the decrease in the surface energy of the melted electrode can probably account for the decrease in the length of the melted electrode with the introduction of O_2 into shielding gas.

4. Numerical Modeling of Metal Transfer

In welding process, the Lorentz force, which is the electromagnetic force by the interaction of the welding current with its own magnetic field, produces the instability of hydromagnetic fluid cylinder as shown in **Fig.7**, and affects the metal transfer modes.

We assume the melted electrode as a fluid cylinder as shown in **Fig.8**. In the radial pinch instability, there is only axial symmetric deformation of the longitudinal profile as shown in Fig.7(a). In the kink instability, the cylinder collapses into a spiral. In the flute instability, perturbations generate a geometry akin to a twisted ribbon and eventually the ribbon splits along the flute which is a longitudinal grooves. The radial pinch and kink instabilities appear in actual welding processes. From the analogy of the shape of the melted electrode observed, we suppose that the globular and axial spray

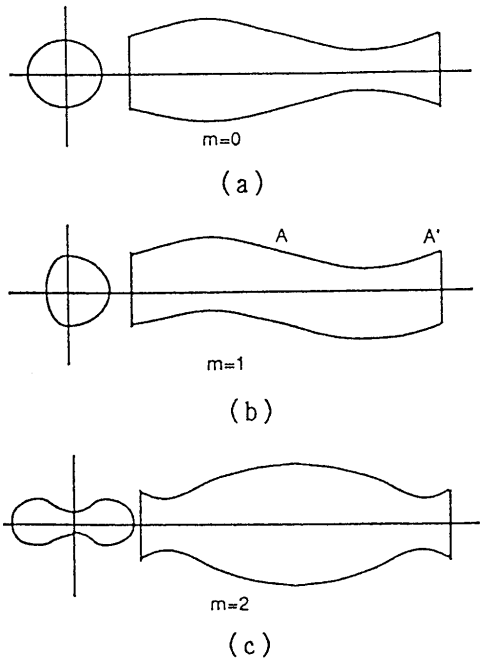

Fig.7 Perturbation of fluid cylinder.
(a) Radial pinch instability
(b) Kink instability
(c) Flute instability

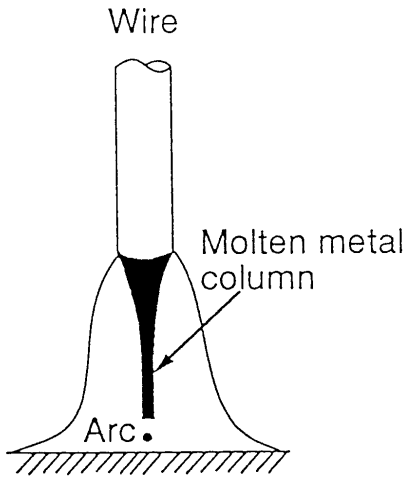

Fig.8 Schematic illustration of ideal melted electrode.

transfers appear, when the effect of the radial pinch instability is dominant, and the rotating spray transfer appears, when the effect of the kink instability is dominant.

We discuss the transition of metal transfer mode by numerical calculation of the dynamics of instability in fluid cylinder[4]. When we apply a perturbation to the fluid cylinder in both the z direction and the θ direction, the profile of the cylindrical surface during perturbation is given by

$$r = R + \varepsilon \cos\left[-m\theta + \left(\frac{2\pi}{\lambda}\right)z\right] \quad (1)$$

and $$\varepsilon = \varepsilon_0 \cos \omega t \quad (2)$$

where R is the radius of the cylinder, λ the wavelength of disturbance, ε the amplitude of disturbance and $\omega/2\pi$ the frequency of disturbance. Here, m determines the instability mode of the cylinder. If m=0, the mode is the radial pinch instability. If m=1, the mode is the kink instability. If m=2, the mode is the flute instability. We ignore viscous force and assume that the pressure is only due to surface tension. Then the governing equations are given by

$$\rho \frac{d\mathbf{v}}{dt} = -\nabla p + \mathbf{J} \times \mathbf{B} \quad (3)$$

$$\nabla \cdot \mathbf{v} = 0 \quad (4)$$

$$\nabla \times \mathbf{B} = \mu_0 \mathbf{J} \quad (5)$$

$$\frac{\partial \mathbf{B}}{\partial t} + \nabla \times \mathbf{E} = 0 \tag{6}$$

$$\mathbf{J} = \sigma(E + \mathbf{v} \times \mathbf{B}) \tag{7}$$

and $$\nabla \cdot \mathbf{B} = 0 \tag{8}$$

where ρ is the mass density, v the fluid velocity, B the magnetic field, E the electric field, μ_0 the magnetic permeability, and σ the electric conductivity. From these governing equations, we finally obtain the dispersion relation between the mode x ($=2\pi R/\lambda$) and the angular frequency of amplitude ω_m under the surface perturbation.

$$\omega_m^2 = \frac{\gamma}{\rho R^3}\frac{xI_m'(x)}{I_m(x)}(x^2 + m^2 - 1) - \frac{\mu_0 I_0^2}{\rho} f(x) \tag{9}$$

$$\Omega^2 = \frac{\rho R^3}{\gamma}\omega_m^2 = \frac{xI_m'(x)}{I_m(x)}(x^2 + m^2 - 1) - \frac{\mu_0 I^2}{\pi^2 R\gamma} f(x) \tag{10}$$

$$f(x) = 1 + \frac{x}{2}\left\{\frac{I_m'(x)}{I_m(x)} - \frac{I_m(x)}{I_m'(x)}\right\} - \frac{m^2 I_m(x)}{xI_m'(x)}\{1 + I_m(x)K_m(x)\} \tag{11}$$

and $$x = \frac{2\pi R}{\lambda} \tag{12}$$

where γ is the surface tension, $I_m(x)$ the modified Bessel function of the first kind of order m, and $K_m(x)$ the modified Bessel function of the second kind of order m.

Assuming that $\rho = 7\times10^3 \mathrm{kg/m^3}$, $\gamma = 1.2\mathrm{N/m}$, R=0.6mm and I=300A, we obtain the calculated results shown in **Fig.9**. When $0<x<8$, the radial pinch (m=0) and kink (m=1) instability are unstable, since $(\rho R^3/\gamma)\omega_m^2 = \Omega^2 < 0$, but the flute instability (m=2) is stable since $\Omega^2 > 0$. In the Ω^2-x curves of all modes (m=0, 1 and 2), Ω^2 has a minimum. When Ω^2 takes the minimum value, the instability grows at a maximum rate. The maximum growth rate of the instability is shown as a function of current in **Fig.10**. The high growth rate means the mode is more predominant. The growth rate of the flute instability (m=2) is much smaller than the radial pinch (m=0) and kink (m=1) instability. This suggests that the flute instability appears very rarely in comparison with the radial pinch and kink instability. This result agrees with the experimental results that the flute instability was not observed in actual welding process. But we can not conclude for this result that the kink instability is the cause of the rotating spray transfer mode since the growth rate of the radial pinch instability (m=0) is larger than that of the kink instability (m=1) as can be seen in Fig.10.

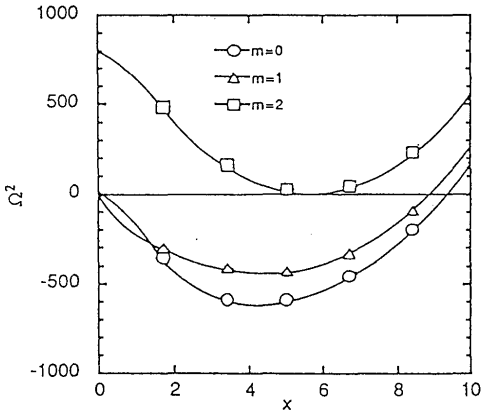

Fig.9 Non dimensional growth rate of instability.

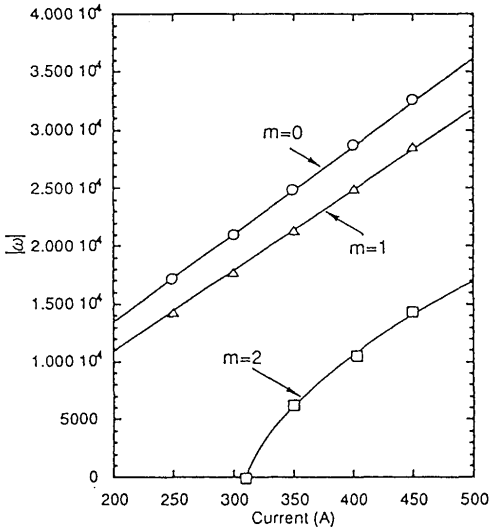

Fig.10 Growth rate of the modes m=0, 1 and 2.

Therefore, we take into account the experimental values of disturbance wavelength λ. The experimental values of λ are listed in **Table 3**. The results calculated from the experimental value of λ are shown in **Fig.11**. When λ for the projected transfer mode is assumed, as shown in Fig.11(a), the growth rate of the radial pinch instability is much higher than that of the kink instability. When λ for the streaming transfer mode is assumed, as shown in Fig.11(b), both radial pinch and kink instability have almost same growth rate. When maximum value λ for the streaming transfer mode is assumed, as shown in Fig.11(c), the growth rate of the kink instability is much higher than that of the radial pinch instability. There results suggest that the length of melted electrode controls the transition of metal transfer modes. If the melted electrode is short, the drop transfer and axial spray transfer predominantly appear due to the radial pinch instability. On the other hand, if the melted electrode is long, the swinging spray transfer and rotating

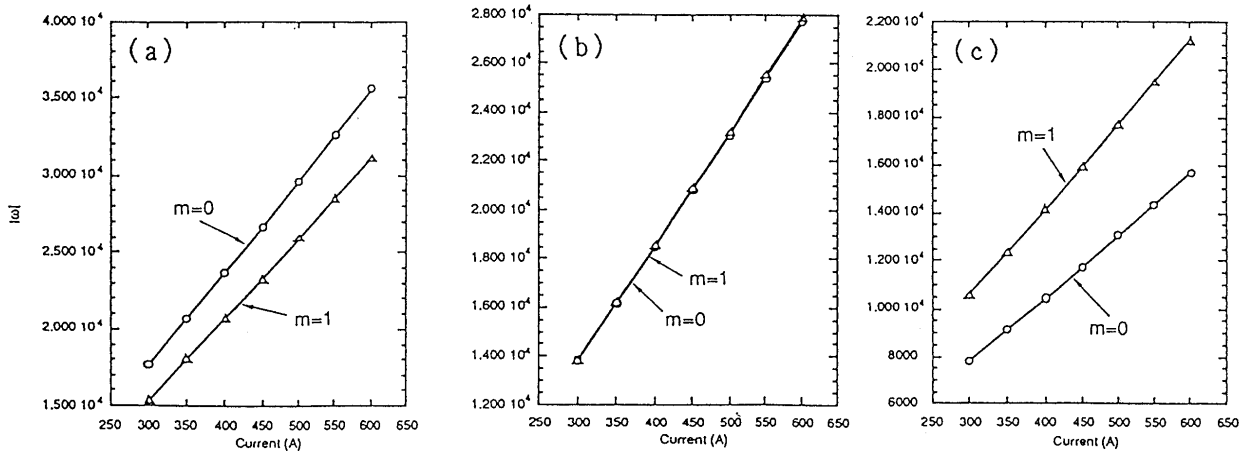

Fig.11 Growth rate of the mode m=0 and m=1 for various wavelength

spray transfer predominantly appear due to the kink instability.

As described in §3.2, when we use Ar+He gas mixture for shielding, the swinging spray transfer mode and rotating spray transfer mode occupied large areas in the transfer mode map. This may be explained by the longer melted electrode and resulting enhancement of the kink instability when Ar+He shielding gas was used.

Table 3 Value of wavelength.

Figure	λ(cm)
(a)	0.183
(b)	0.277
(c)	0.554

The introduction of O_2 into Ar+He gas mixture increased the area of axial spray transfer mode and decreased the area of swinging spray transfer mode. This result may also be explained by the disturbance wavelength λ, since the length of melted electrode was decreased as O_2 was introduced into shielding gas.

In the transfer mode map of Ar+CO_2 gas mixture for shielding, the welding current at the boundaries between the transfer modes was increased with the mixture ratio of CO_2. This result can be explained as follows: since the end of the melted electrode is held up by the arc force, the effective length of melted electrode becomes short as the mixture ratio of CO_2 is increased, and the modes associated with shorter disturbance wavelength become more predominant.

5. Conclusion

(1) Metal transfer modes in the high current GMA welding are roughly classified into four types depending on the welding current: globular transfer, axial spray transfer, swinging spray transfer and rotating spray transfer. The globular transfer is further classified into drop transfer and repelled transfer. The axial spray transfer is further classified into projected transfer, streaming transfer and repelled spray transfer.

(2) The length of melted electrode control the transition of metal transfer modes. When the melted electrode is short, drop transfer and axial spray transfer predominantly appear due to the radial pinch instability. On the other hand, when the melted electrode is long, swinging spray transfer and rotating spray transfer predominantly appear due to the kink instability. The experimental results support that the effect of the shielding gas composition on the transfer modes can be explained by the length of the melted electrode.

References

1) J.R.Matthews, J.F.Porter, J.Church and M.Macecek : An Evaluation of TIME Welding of HY80 Plate, Welding Journal, Vol.70 (1991), No.2, 35-41

2) H.Yamamoto, S.Harada and Y.Yamamoto : Japan Welding Technique, Vol.38 (1990), No.2, 68-85 (in Japanese)

3) S.Z.Beer : Liquid Metals Chemistry and Physics, Marcel Dekker, New York (1972)

4) J.F.Lancaster : The Physics of Welding, Pergamon Press (1984), Capter 3